

[Neuroscience](#). Author manuscript; available in PMC 2010 Oct 20.

PMCID: PMC2765788

Published in final edited form as:

NIHMSID: NIHMS137986

[Neuroscience](#). 2009 Oct 20; 163(3): 877–889.

PMID: [19596056](#)

Published online 2009 Jul 24. doi: [10.1016/j.neuroscience.2009.07.012](#)

## STRIATAL NEUROPROTECTION WITH METHYLENE BLUE

[Julio C. Rojas](#),<sup>a</sup> [Nicola Simola](#),<sup>b</sup> [Bailey A. Kermath](#),<sup>a</sup> [Jacqueline R. Kane](#),<sup>c</sup> [Timothy Schallert](#),<sup>a,c,d</sup> and [F. Gonzalez-Lima](#)<sup>a,c,e</sup>

### Abstract

---

Recent literature indicates that low-dose methylene blue (MB), an autoxidizable dye with powerful antioxidant and metabolic enhancing properties, might prevent neurotoxin-induced neural damage and associated functional deficits. This study evaluated whether local MB may counteract the anatomical and functional effects of the intrastriatal infusion of the neurotoxin rotenone in the rat. To this end, stereological analyses of striatal lesion volumes were performed and changes in oxidative energy metabolism in the striatum and related motor regions were mapped using cytochrome oxidase histochemistry. The influence of MB on striatal levels of oxidative stress induced by rotenone was determined, and behavioral tests were used to investigate the effect of unilateral MB co-administration on motor asymmetry. Rotenone induced large anatomical lesions resembling “metabolic strokes”, whose size was greatly reduced in MB-treated rats. Moreover, MB prevented the decrease in cytochrome oxidase activity and the perilesional increase in oxidative stress associated with rotenone infusion in the striatum. MB also prevented the indirect effects of the rotenone-induced lesion on cytochrome oxidase activity in related motor regions, such as the striatal regions rostral and caudal to the lesion, the substantia nigra compacta and reticulata, and the pedunculopontine nucleus. At a network level, MB maintained a global strengthening of functional connectivity in basal ganglia-thalamocortical motor circuits, as opposed to the functional decoupling observed in rotenone-alone subjects. Finally, MB partially prevented the behavioral sensorimotor asymmetries elicited by rotenone. These results are consistent with protective effects of MB against neurotoxic damage in the brain parenchyma. This study provides the first demonstration of the anatomical, metabolic and behavioral neuroprotective effects of MB in the striatum *in vivo*, and supports the notion that MB could be a valuable intervention against neural damage associated with oxidative stress and energy hypometabolism.

**Keywords:** Cytochrome oxidase, Methylthioninium chloride, Mitochondria, Parkinson disease, Rotenone, Stroke

---

Methylene blue (MB) is a Food and Drug Administration-grandfathered autoxidizable phenothiazine with potent antioxidant and metabolic enhancing properties at low doses ([Bruchey and Gonzalez-Lima, 2008](#)). MB has been widely used as a supravital stain of nervous tissue ([O'Leary et al., 1968](#)), as well as an artificial electron donor ([Lindahl and Oberg, 1961](#), [Lehninger, 1964](#), [Scott and Hunter, 1966](#)). Its major use in pharmacotherapy is as an antidote for metabolic poisons that induce methemoglobinemia ([Clifton and Leikin, 2003](#)). MB readily crosses the blood-brain barrier and has a high bioavailability to the brain ([Peter et al., 2000](#), [Wainwright and Crossley, 2002](#)). Experimentally, MB has been shown to prevent the signs of hypoxia-induced neuronal injury and systemic oxidative stress in a pig model of controlled cardiac arrest ([Miclescu et al., 2006](#)), and has been used to effectively treat and prevent encephalopathy in humans undergoing cancer chemotherapy with ifosfamide ([Kupfer et al., 1994](#), [Kupfer et al., 1996](#), [Pelgrims et al., 2000](#)). Furthermore, the effects of chronic MB therapy on progression of Alzheimer's disease, a disorder associated with mitochondrial dysfunction, are currently being tested in clinical trials ([Wischik et al., 2008](#)), and there is evidence that MB is safe when administered chronically for the treatment of mental disorders in humans ([Naylor et al., 1986](#)).

*In vivo* preclinical studies have confirmed the beneficial properties of MB on neuronal function by demonstrating that at small doses, it is capable of preventing the deleterious neurobehavioral effects induced by the administration of neurotoxins. For example, systemic MB prevented learning deficits and the spatial memory impairment elicited in rats by sodium azide ([Callaway et al., 2002](#)). MB also reduced the latency to seizure onset and prevented the electroencephalographic changes induced in rats by the intrastriatal administration of methylmalonate ([Furian et al., 2007](#)). Finally, in a rodent model of optic neuropathy, MB prevented the visual impairment and structural retinal damage caused by the intravitreal administration of the neurotoxin rotenone (Rot) ([Zhang et al., 2006](#), [Rojas et al., 2009](#)). This latter finding appears of particular interest as it revealed potent neuroprotective effects of MB in an experimental paradigm of neurotoxin-induced neurodegeneration. Based on this, MB might also prove effective in reducing neurotoxic structural and functional damage in the brain parenchyma.

To test this hypothesis, the present study evaluated whether local MB co-administration would reduce the neurotoxic effects elicited by Rot selectively infused in the striatum. The striatum was targeted because striatal damage is an important pathophysiologic component of neurodegenerative motor disorders ([Villalba et al., 2009](#)). Previous studies have demonstrated that Rot induces severe neurodegeneration associated with motor functional impairment in the rat, when selectively infused into brain regions such as the striatum ([Sindhu et al., 2006](#)), the medial forebrain bundle ([Alam et al., 2004](#), [Sindhu et al., 2005](#)) or the substantia nigra ([Saravanan et al., 2005](#)). In this study, the neuroprotective effects of MB were investigated using two variations of the same rat model of striatal neurotoxicity, involving either unilateral or bilateral Rot-induced striatal lesions. Lesions were analyzed through stereological methods, and functional differences between Rot and Rot/MB-treated subjects were assessed by comparing regional- and network-level changes in brain oxidative energy metabolism ([Sakata et al., 2005](#)), and by sensorimotor asymmetry tests sensitive to striatal injury ([Schallert, 2006](#)).

## EXPERIMENTAL PROCEDURES

---

### Subjects and chemicals

Male Sprague-Dawley rats ( $n = 55$ , average weight  $407 \pm 35$  g) were obtained from Harlan (Houston, TX). Subjects were handled daily to allow for habituation. They were maintained in clear polycarbonate cages (3 per cage) with food and water *ad libitum* and subjected to standard light cycles (12 hr light/12 hr dark, 0 lights on at 07:00 am) in a facility accredited by the Association for the Assessment of Laboratory Animal Care International. All experimental procedures were approved by the Institutional Animal Care and Use Committee of the University of Texas at Austin. MB (1% solution USP grade pure, preservative free) was purchased from Faulding Pharmaceuticals (Aguadilla, PR). Isoflurane was purchased from Baxter (Deerfield, IL). Unless otherwise specified, additional chemical reagents were purchased from Sigma-Aldrich (St. Louis, MO).

### Intrastriatal rotenone infusion and tissue processing

General anesthesia with isoflurane was induced at 3% for 3 min and maintained at 1.5–3% using an E-Z anesthesia vaporizer system (Euthanex, Corp, Palmer, PA). Animals were placed in a stereotaxic apparatus and their skull exposed by a mid-sagittal incision. Trephinations were done at stereotaxic coordinates +0.3 mm A-P and +3.0 mm L, relative to Bregma level ([Paxinos and Watson, 1997](#)). A 30-G dental microinjection needle (Monoject®, Sherwood Medical Company, Norfolk, NE) was slowly lowered through the burr hole to a depth of 5 mm ventral to the dura targeting the central portion of the striatum. The needle was connected by polyethylene tubing (internal diameter = 0.38 mm) to a 10  $\mu$ L Hamilton microsyringe. Each rat was infused with dimethylsulfoxide (DMSO), 12  $\mu$ g Rot or 12  $\mu$ g Rot plus 8.8  $\mu$ g methylene blue (Rot/MB). The Rot dose was based on pilot experiments and previous studies showing effective and reproducible nigrostriatal degeneration ([Saravanan et al., 2005](#), [Sindhu et al., 2005](#)). The MB dose was based on a previous dose-response study showing neuroprotective effects against Rot-induced neurodegeneration in the retina ([Zhang et al., 2006](#)). DMSO was used as a vehicle for intrastriatal infusions. In this vehicle Rot/MB solutions are stable and the two compounds do not interact with each other ([Zhang et al., 2006](#), [Rojas et al., 2009](#)). Fresh solutions were prepared every day. Each infusion was delivered over 2 min using a microinjection pump (CMA microdialysis AB, North Chelmsford, MA) (flow rate 1  $\mu$ L/min; 2  $\mu$ L, final volume) and the injection needle was left in place for an additional 3 min period to allow for diffusion away from the needle tip. The needle was then slowly retracted to avoid any leaking through the needle tract.

In a unilateral lesion model, 22 rats were used as follows: 4 subjects were infused with the vehicle DMSO into the left striatum, 9 subjects were infused Rot into the left striatum, and 9 subjects received infusions of Rot/MB into the left striatum. The incision was sutured with 2-0 nylon thread and the rats were allowed to recover on heated cages before being returned to their home cages. One subject in the Rot group was decapitated 1 hr after surgery. The rest of the subjects were decapitated seven days after surgery. Eleven additional rats were used in a model of bilateral striatal lesions, in which each subject received Rot in the left striatum and Rot/MB in the right striatum. All animals in the bilateral lesions model were decapitated seven days after surgery. The brains of all subjects were collected and slowly frozen in  $-40^{\circ}\text{C}$  isopentane. Coronal brain sections (40  $\mu$ m-thick) were obtained in a 2800 Frigocut E Reichert-Jung cryostat (Leica Microsystems, Bannockburn, IL) at  $-18^{\circ}\text{C}$  and were mounted on glass slides to create three adjacent series for histological analysis. Sections were stored at  $-40^{\circ}\text{C}$  until further use.

### Nissl staining

Frozen brain sections were delipidized in a series of 95% ethanol, 70% ethanol, distilled water, and 0.1 M sodium acetate buffer at pH 4 (2.5 min each). Sections were stained in 0.1% cresyl violet in sodium acetate buffer at 45°C for 7 min, differentiated in 70% and 95% ethanol and dehydrated in 95% and 100% ethanol. Slides were cleared in xylene and coverslipped with Permount®.

### Striatal oxidative stress

Dihydroethidium (DHE) fluorescence was used to determine the *in situ* levels of oxidative stress in unfixed frozen brain sections as described previously ([Rojas et al., 2008b](#)). On-the-slide brain sections were incubated in 10 µM DHE (Invitrogen, Carlsbad, CA) in PBS, pH 7.4, for 30 min at 37°C in the dark. Excess fluid was removed and slides were coverslipped with ProGold® antifading medium (Invitrogen, Carlsbad, CA). Images were captured with an epifluorescence microscope (BX61, Olympus, Center Valley, PA) at  $\lambda = \text{Ex: } 490, \text{Em: } 520 \text{ nm}$ , magnification: 50X, and with similar camera acquisition settings and exposure times for all sections. Regions of interest consisted of the medial striatum in unimpaired hemispheres and striatum immediately lateral to the lesions in infused hemispheres. Digital images were analyzed for densitometry with Image J software (NIH). Data are expressed as the ratio of mean total gray values pixel counts.

### Cytochrome oxidase activity histochemistry

Brain sections were stained with Wong-Riley's histochemical method ([Wong-Riley, 1979](#)) modified for the quantitative measurement of cytochrome oxidase activity in fresh-frozen sections as previously described ([Gonzalez-Lima and Cada, 1994](#), [Gonzalez-Lima and Jones, 1994](#), [Gonzalez-Lima and Cada, 1998](#)).

Fresh-frozen sections were submerged in 0.5% glutaraldehyde/10% sucrose in PB, pH 7.6, for 5 min at 4°C, followed by three baths of 10% sucrose in PB (5 min each, allowing for gradual increases in temperature). The sections were incubated for 10 min in a solution containing 50 mM Tris, 1.1 mM cobalt chloride, 10% sucrose and 0.5% DMSO. After a 5 min rinse in PB at room temperature, the sections were stained for 60 min at 37°C in a PB solution containing 1.3 mM 3,3'-diaminobenzidine tetrahydrochloride, 75 mg/L cytochrome *c*, 20 mg/L catalase, 5% sucrose and 0.25% DMSO. Sections were fixed in 10% formalin in PB at room temperature for 30 min, dehydrated in series of 30%–100% ethanol series, cleared in xylene (2 times, 5 min each) and coverslipped with Permount®.

### Complex I histochemistry

Brain tissue was stained for mitochondrial complex I [nicotinamide adenine dinucleotide (NADH) dehydrogenase] activity as described previously ([Jung et al., 2002](#), [Zhang et al., 2002](#)). Fresh-frozen sections were pre-fixed in a solution containing 0.5% glutaraldehyde and 10% sucrose in phosphate buffer (PB) for 7 min at room temperature, followed by 10% sucrose in PB baths (3 times, 5 min each). The sections were incubated at 37°C for 15 min with gentle agitation in PB containing NADH (1 mg/ml), nitroblue tetrazolium (1.33 mg/ml), and 1 M sodium azide. After this, sections were rinsed in PB, fixed in 10% paraformaldehyde for 30 min at room temperature, dehydrated in alcohol series, cleared in xylene and coverslipped with Permount®.

### Morphometry

Total striatal volumes and lesion volumes were estimated using the Cavalieri principle by an investigator blind to the groups. Images of Nissl-stained brain sections were digitized using JAVA imaging software (Jandel Scientific; Corte Madera, CA). Regions of interest were delineated and their areas calculated in six to twelve samples, depending on the size of the lesion, at uniform intervals starting where the striatum was first visible in the rostro-caudal plane at approximate coordinates from Bregma = +1.7 ([Paxinos and Watson, 1997](#)). Areas (A) were used together with d, the average distance between designated sections, to estimate the total striatal volume as well as lesion volume, based on the formula  $V_{\text{striat}} = \sum A \times d$ . The value d was calculated as  $d = (T) \times (\text{number of designated sections}-1) \times (\text{number of series})$ , where T is the distance between every designated section (380  $\mu\text{m}$ ).

### Brain metabolic mapping

Brain maps of cytochrome oxidase activity were obtained by an investigator blind to the groups through a well-established method of optical densitometry of brain sections as detailed by [Gonzalez-Lima and Cada \(1994\)](#). A calibration step tablet (density range 0.05–3.05) and cytochrome oxidase activity-stained sections were placed on a DC-powered light box and digitized using a CCD camera (Javelin Electronics; Torrance, CA) and a Targa-M8 digitizer. Digitized images were analyzed for optical density using the “intensity” or “average intensity” functions of JAVA imaging software (Jandel Scientific; Corte Madera, CA). This software allows creating a logarithmic calibration curve of optical density units as a function of pixel (gray level) values in each image. Before analysis, images were corrected for slide and light box artifacts using background subtraction. For brain structures, sampling box sizes were adjusted to sample most of the region of interest with four readings per hemisphere per animal. The median of optical density values for each region of interest were converted to units of cytochrome oxidase activity using calibration curves based on standards of tissue thickness and spectrophotometrically-determined cytochrome oxidase activity. For this purpose, cryosections of a frozen pool of rat brain homogenates ( $n = 10$ ) were cut at different thicknesses (10, 20, 40, 60 and 80  $\mu\text{m}$ ) to obtain increasing gradients of cytochrome oxidase reactivity. This method yielded a linear relationship ( $r > 0.95$ ) between biochemical cytochrome oxidase activity units measured by spectrophotometry and histochemical cytochrome oxidase reactivity measured by optical density. Group comparisons were made based on cytochrome oxidase activity values.

Areas of interest ipsilateral and contralateral to the lesion included: 1) rostral striatum (CPuR), 2) caudal striatum (CPuC), 3) lateral globus pallidus (LPG), 4) subthalamic nucleus (STh), 5) substantia nigra reticulata (SNr), 6) substantia nigra compacta (SNc), 7) pedunculopontine nucleus (PPTg), 8) ventrolateral thalamic nucleus (VL), 9) ventral anterior thalamic nucleus (VA), 10) centromedian thalamic nucleus (CM), 11) primary motor cortex, 12) secondary motor cortex (M2), 13), primary somatosensory cortex, 14) medial orbital cortex (MO), 15) medial frontal cortex (MFC) and 16) anterior cingulate cortex (ACC). Cytochrome oxidase activity was reported as  $\mu\text{mol}/\text{min}/\text{g}$  of wet tissue. A similar imaging method was followed to analyze complex I activity-stained sections. Complex I activity values were determined spectrophotometrically as detailed below, and they were used together with optical density curves derived from standards of tissue thickness (5–60  $\mu\text{m}$ ) that yielded a linear correlation with optical density values ( $r = 0.97$ ). *In situ* total striatal complex I activity was derived from optical density values in subjects from the unilateral lesion model.

Cytochrome oxidase activity was used as a marker of neuronal metabolic activity ([Wong-Riley, 1989](#)) in the striatum at the lesion level, taking into account the potential presence of a lesion penumbra. For the purposes of the present study, the penumbra was defined as a transition zone between injury and repair that represents a mismatch between a larger area of anatomic damage and a smaller zone of hypometabolism. For sampling purposes, four arbitrary eccentric zones were defined within the lesion, including: 1) core, defined as the zone with the lowest cytochrome oxidase activity within the striatum and that contained the region with the most severe anatomical damage; 2) inner penumbra, immediately adjacent to the core within a 0.028 mm<sup>2</sup> sample frame; 3) outer penumbra, adjacent to the inner penumbra within a 0.028 mm<sup>2</sup> sample frame, and 4) spared striatum, which included the rest of the striatum not affected by the lesion.

In order to assess the system-level changes in metabolic activity, the cytochrome oxidase activity data were applied to a basal ganglia-thalamocortical circuit defined by anatomic connectivity as proposed by [Alexander et al. \(1990\)](#). Patterns of functional connectivity were determined based on a covariance analysis of interregional metabolic activity. In modeling approaches like this, the network functional connectivity is not based on excitatory or inhibitory electrophysiological relationships between regions in terms of neurotransmission, but on functional interactions that determine the magnitude and direction of the covariance pattern of interactivity between regions ([McIntosh and Gonzalez-Lima, 1991](#), [Sakata et al., 2000](#)). A model based on cytochrome oxidase activity expresses how a change in metabolic activity in a specific region is associated with an increase or decrease of metabolic activity in other region(s), thus providing an overview of the functional coupling between regions in terms of energy-dependent metabolic capacity ([Sakata et al., 2000](#)). This covariance approach is useful in identifying group differences that would not be evident using univariate statistical comparisons of regional metabolic activity, and it has been implemented in several human neuroimaging studies of the basal ganglia in young subjects, aged subjects and patients with Parkinson's disease ([Grafton et al., 1994](#), [Taniwaki et al., 2006](#), [2007](#)).

### Complex I activity in striatal mitochondria

Twelve additional rats were used in which striatal mitochondria were isolated as described previously ([Rojas et al., 2009](#)). Striata from twelve fresh rat brains were dissected and homogenized in ice-cold suspension (10 mM MES, 200 mM mannitol, 70 mM sucrose, 1 mM EGTA, and 0.02% delipidated BSA, pH 7.5) (1:10 wt/vol) using a 7 ml Dounce glass homogenizer (10–15 strokes per brain), and the tissue was centrifuged at 1000 × g at 4°C for 5 min. The supernatant was centrifuged again at 3500 × g at 4°C for 15 min, and the pellet resuspended in 1 mL of ice-cold suspension for further centrifugation at 1000 × g at 4°C for 5 min. The supernatant centrifugation step was repeated and the remaining pellet was resuspended (40 µL per 100 mg of tissue), assayed for protein concentration, and stored at –40°C until use. Freeze-thaw cycles were avoided. Complex I activity measurements were based on the detection of NADH oxidation, as described previously ([Estornell et al., 1993](#)). Mitochondria (1 µg/mL) were diluted in reaction buffer (250 mM sucrose, 1 mM EDTA, 50 mM Tris-HCl, pH 7.4) with 10 µM decylubiquinone, 2 mM sodium azide, 2 µM antimycin A. The reaction was started by adding 75 µM NADH, which oxidation was followed spectrophotometrically by the decrease of absorbance at 340 nm for 3 min at 30°C ( $\epsilon = 6.75 \text{ mM}^{-1} \text{ cm}^{-1}$ ). Rot (2 µM) or Rot plus MB (0.5–50 µM) were added in subsequent experiments to approximate concentrations reached in intrastriatal infusions. For an average lesion volume of 42 mm<sup>3</sup> in Rot-infused hemispheres, the final estimated Rot concentration in the animal model approaches 1 µM. Similarly, the estimated MB concentration is about 0.5 µM. All experiments were done at least in triplicate.

## Behavioral tests

Subjects in the unilateral lesion model underwent two behavioral tests previously demonstrated to effectively detect the presence of motor asymmetries in rats bearing a unilateral neurotoxic insult ([Schallert et al., 1982, 1983, 1986](#), [Barth and Stanfield, 1994](#), [Schallert et al., 2000](#), [Schallert and Woodlee, 2005](#), [Woodlee et al., 2005](#)). These tests included 1) a somatosensory asymmetry (dot removal) test, and 2) a vibrissae-evoked forelimb placing test. The tests were performed before and after surgery by experienced testers blind to the treatment conditions and at similar times between days. Before surgery each test was performed twice and results were averaged to establish baseline parameters. After surgeries each test was performed a first time on post-lesion day 3 and repeated on post-lesion day 7. Methods for each behavioral test used are detailed below.

**Dot removal test** Neurologically intact rats are able to contact and promptly remove external stimuli (e.g. a small dot of adhesive tape) placed by an experimenter on their forelimb(s). An increase in the latency to contact and remove the stimuli can be used as an indicator of neurological deficit ([Schallert et al., 1982, 1983](#), [Fleming et al., 2005](#)). The dot removal test used in this study consisted of three trials during which, one Tough Spot circular adhesive-backed label (81 mm<sup>2</sup>) (Diversified Biotech, Boston, MA) was placed on the distal-radial aspect of each forelimb in a random order. After dot placement, each rat was returned to its cage and the order and latency of dot contact as well as removal for each forelimb was recorded.

**Vibrissae-evoked forelimb placing** Neurologically intact rats are known to readily place their forelimb on a hard surface in response to tactile vibrissae stimulation (e.g. gently brushing of the vibrissae against a table edge), but this response may be lost following certain types of brain injury ([Barth and Stanfield, 1994](#), [Hua et al., 2002](#), [Schallert and Woodlee, 2005](#)). In the present study, vibrissae-evoked forelimb placing was performed by holding each rat aloft and gently brushing either its left or its right vibrissae against the edge of a tabletop to trigger a placing response in the forelimb ipsilateral to the stimulated vibrissae. The test was scored in a nominal scale from 0 to 3, where 0 = no movement, 1 = limb movement with no surface contact, 2 = incomplete contact, 3 = complete contact ([Anstrom et al., 2007](#)). Each limb was scored independently and results were expressed as the mean placing score of ten trials for each limb.

**Open field activity** Open field activity measures were obtained to screen for differences in gross motor behavior. This test was performed by individually placing each rat in a predetermined corner of an open field chamber and then recording its spontaneous behavior for 10 minutes. The chamber (43.2 cm<sup>2</sup>) had clear plastic sides 30.5 cm high and a white Plexiglas floor. Arrays of infrared light beam motion detectors (16 × 16, 2.5 cm apart) were placed at the sides of the chamber, thus creating a detection grid. Two arrays of detectors were located 1 cm above the floor, and another array was located 13 cm above the floor, to detect rearing. The chambers were controlled by the Activity Monitor program, version 5.10 (Med Associates, St. Albans, VT). To ensure the absence of olfactory cues, which may influence rats' motor activity, chambers were washed with diluted Bio-clean® solution between each session. Measures of motor activity included: ambulatory distance, short movement, rearing time, immobility time and average velocity, which were automatically scored by a computer using MED-PC software.

## Statistical analysis

Within-subject (left vs. right hemisphere) comparisons of striatal volumes, lesion volumes, regional cytochrome oxidase activity and DHE signal were performed by means of two-tailed paired samples t-tests. Between-subject group comparisons for these variables were conducted with Dunnett test-corrected analysis of variance (ANOVA). The striatal cytochrome oxidase activity in the lesioned hemisphere in proportion to that of the contralateral striatum was obtained along the rostro-caudal axis and treatment comparisons were done with the Mann-Whitney U test. Zonal analyses of cytochrome oxidase activity of lesions in the unilateral lesion model (group x lesion zone) were done with factorial ANOVA with staining batch as a covariate. Differences in interregional functional interactions were calculated according to the method of [Jones and Gonzalez Lima \(2001\)](#). Pearson correlations between cytochrome oxidase activity in the regions of interest were obtained. Each correlation was then converted by the Fisher Z-transformation into a number whose distribution is approximately normal and has an expectation  $E_{(Z)} = 0.5 \log [(1 + \rho_{XY}) / (1 - \rho_{XY})]$  and variance:  $\text{Var}(z) = 1 / (N \pm 3)$ , where  $\rho_{XY}$  is the population correlation coefficient between variable X and Y and N is the sample size. These correlations were tested for significant differences between groups. The Fisher Z transformation was used to convert each correlation to a Z score. A test statistic of the form

$$Z = \frac{Z_{ij(\text{group1})} - Z_{ij(\text{group2})}}{\sqrt{(1/n_{g1} - 3) + (1/n_{g2} - 3)}}$$

(where  $Z_{ij}$  is the Fisher Z transformation value for the correlation coefficient between regions  $i$  and  $j$ ,  $n_{g1}$  is the sample size in group one, and  $n_{g2}$  is the sample size in group two) was used to compare group differences. Two correlations were considered significantly different when the Fisher Z transformation value was higher than 1.96 (two standard deviations). Within-subject comparisons in behavioral performance before and after the surgeries were analyzed with the Wilcoxon signed ranks test. Between-group comparisons in behavioral performance were done with the Mann-Whitney U test. *In situ* complex I activity mean values were compared with two-tailed paired or unpaired t tests, and differences in percent changes in complex I activity were done with the Mann-Whitney U test. Means of complex I activity in striatal mitochondria were compared using Dunnett-corrected one-way ANOVA. All statistical analyses were conducted using SPSS 11.5 for Windows. A two-tailed p value < 0.05 was considered significant.

## RESULTS

---

### Rotenone infusion in the striatum resulted in an early metabolic lesion

Rot-induced striatal damage was preceded by regional energy hypometabolism, since the striatum showed a decrease in cytochrome oxidase activity in the absence of gross neurodegeneration at 1 hr after Rot-infusion. The ipsilateral/contralateral striatal cytochrome oxidase activity ratio was 21% lower in the Rot-infused subject than control ( $p < 0.01$ ). Nissl staining of the Rot-infused striatum at the same Bregma level where hypometabolism was detected showed only mild ipsilateral ventricular enlargement but no clear gliosis or major structural damage ([Fig 1A and 1B](#)). Vehicle only-treated striata showed no visible signs of hypometabolism or gross structural lesions ([Fig 1C and 1D](#)).

## [Figure 1](#)

### **Energy hypometabolism precedes striatal neurodegeneration**

(A) A Nissl-stained rat brain coronal hemisection at Bregma level +0.3 mm shows very little evidence of ipsilateral striatal structural damage 1 hr post-Rotenone (Rot) infusion. Only mild hydrocephalus was detected (arrow). (B) At 1 hr, however, cytochrome oxidase activity histochemistry revealed an area of striatal hypometabolism (asterisk) at the same Bregma level in the same subject. (C and D) No evidence of structural lesion or striatal hypometabolism was evident in vehicle-treated subjects after 7 days. Scale bar = 1 mm.

### **MB had structural neuroprotective effects on the striatum**

One week after infusions the Rot-injected hemispheres displayed wide striatal lesions featuring a centrally located area of liquefactive necrosis surrounded by reactive gliosis and accompanied by ipsilateral hydrocephalus and damage to the dorsally located corpus callosum ([Fig. 2A](#)). MB co-administration showed structural neuroprotective effects in the unilateral striatal lesion induced by Rot. The Rot-induced structural damage appeared to be considerably attenuated in the Rot/MB-treated hemispheres ([Fig. 2B](#)). In the lesion size morphometric comparisons, the vehicle-treated control group showed only small areas of reactive gliosis and parenchymal damage (striatal lesion size of  $6.9 \pm 1 \text{ mm}^3$ ). In contrast, the mean lesion volume in Rot-treated hemispheres was  $51.6 \pm 15 \text{ mm}^3$ , which was a significant effect as compared to control hemispheres ( $p < 0.05$ ). In the Rot/MB group, a mean lesion volume of  $24.2 \pm 5 \text{ mm}^3$  was observed. This represents a 53% difference in striatal damage between the Rot/MB group compared to the Rot group. This resulted in a significantly greater amount of spared striatal volume in the Rot/MB group ( $443.3 \pm 16 \text{ mm}^3$ ) than in the Rot group ( $367.3 \pm 21 \text{ mm}^3$ ) ( $p < 0.05$ ).

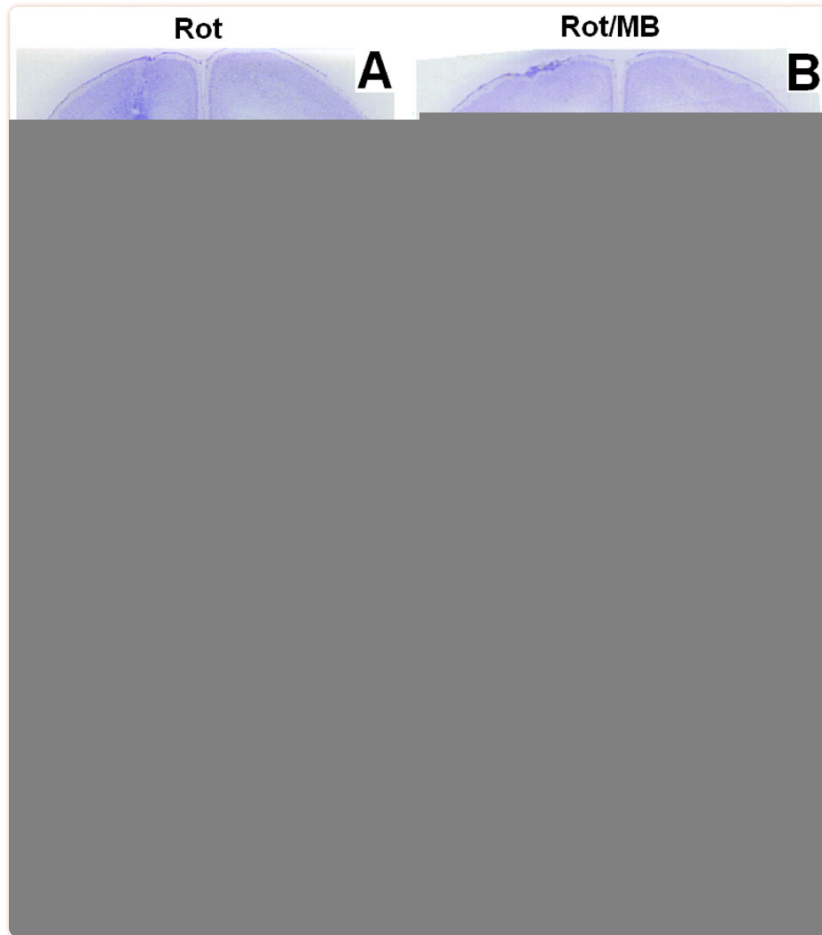


[Figure 2](#)

**Effects of methylene blue on rotenone-induced striatal damage in unilaterally infused rats**

(A and B) Intrastratial infusion of rotenone alone (Rot) produced a large area of liquefactive necrosis surrounded by gliosis (asterisk) and accompanied by mild ipsilateral lateral ventricle enlargement (arrow). The toxic effects of Rot appeared to be attenuated in those rats receiving a combined intrastratial infusion of Rot/MB. (C and D) Peri-lesional oxidative stress *in situ* was measured in micrographs of DHE-stained sections. An increased signal was detected in the striatum adjacent to the lesion in the Rot-treated subjects. Conversely, the DHE signal was comparatively lower in penumbral regions in Rot/MB-treated subjects. Epifluorescence microscopy, 50X. (E and F) Cytochrome oxidase histochemistry-stained fore-brain coronal sections from the same subjects depicted in A and B show corresponding regions of striatal hypometabolism that is less severe in the Rot/MB-treated subject.

**MB had metabolic neuroprotective effects on the striatum**

In a rostro-caudal analysis of the ipsilateral striatal metabolism, areas of decreased activity were detected between Bregma levels 0.7 mm and 0.3 mm in the Rot and Rot/MB groups. The majority of the lesions were contained between these two Bregma levels. In both groups, the striatum between these Bregma levels showed an approximate 11% decrease in cytochrome oxidase activity compared to the striatum at Breg-

ma levels 1.2 mm and  $-0.3$  mm ( $p < 0.05$  and  $p < 0.001$ , respectively). However, between Bregma levels 0.7 mm and 0.3 mm, the area of striatal metabolic depletion in the Rot-treated hemisphere was visibly larger than that of the Rot/MB-treated ones ([Fig. 2E, 2F](#)).

### MB prevented the increase in oxidative stress in the penumbra

In Rot-treated subjects, an average 14.8% increase in the oxidative stress levels was observed in the penumbral region as compared to the contralateral striatum ( $p < 0.05$ ). MB co-administration prevented this increase in oxidative stress, as only a 2.1% increase in levels of oxidative stress were detected in the ipsilateral striatum, relative to the contralateral striatum in the Rot/MB-treated group ([Fig. 2C, 2D](#) and [Fig. 3](#)).

#### [Figure 3](#)

##### **Methylene blue coadministration attenuates the penumbral striatal oxidative stress elicited by intrastriatal rotenone**

In the unilateral lesion model, the perilesional DHE signal observed in the rotenone (Rot)-treated hemispheres (ipsilateral) was significantly higher than that of non-treated hemispheres (contralateral), whereas no interhemispheric difference was observed in the Rot/MB group. \* = different from contralateral striatum,  $p < 0.05$ .

### MB maintained striatal cytochrome oxidase activity in the lesion core

A more detailed analysis of the zone of highest metabolic impairment revealed further significant between-group differences. Compared to control, Rot induced a 52.3% reduction in cytochrome oxidase activity at the site of infusion, which corresponds to the lesion core ( $p < 0.01$ ). In contrast, the decrease in metabolic activity in the Rot/MB group was only 23.9% compared to control ( $p = 0.23$ ). Nevertheless, the Rot/MB group showed a decrease in cytochrome oxidase activity in the penumbra ( $-18\%$ ,  $p < 0.05$ ) and the contralateral striatum ( $-18.6\%$ ,  $p < 0.01$ ) compared to control ([Fig. 4](#)).

#### [Figure 4](#)

##### **Effects of methylene blue co-administration on rotenone-induced hypometabolism in the striatum**

At Bregma level 0.3 mm, the striatum (CPu) in the infused hemisphere was subdivided in three zones: a) lesion core, which matched the region of highest structural damage in Nissl-stained sections, b) lesion penumbra, and c) spared ipsilateral striatum. MB co-administration counteracted the hypometabolism in the striatal lesion core induced by rotenone (Rot). MB also prevented the compensatory changes in metabolic activity caused by Rot in the lesion penumbra and the contralateral striatum (Contra). Ipsi = spared ipsilateral striatum. \* =  $p < 0.05$ .

## MB did not directly increase striatal complex I activity *in vivo* or *in vitro*

The ipsilateral striatum in Rot-treated subjects showed a 21% decrease in total mitochondrial complex I activity, relative to the contralateral striatum ( $p < 0.01$ ), whereas there were no significant interhemispheric differences in cytochrome oxidase activity in this group. This supports a specific inhibitory effect of Rot on complex I activity, as opposed to a more general and unspecific inhibitory action on mitochondrial function. A significant interhemispheric difference in complex I activity was also observed in the Rot/MB group, where the ipsilateral striatum showed a 14.9% decrease, relative to the contralateral striatum. MB co-administration did not increase total striatum complex I activity in the ipsilateral hemisphere in the Rot/MB group, which supports that MB does not directly increase complex I activity, and does not block Rot binding site at complex I. On the other hand, total ipsilateral striatal cytochrome oxidase activity was boosted by 18% in the Rot/MB group, compared to the contralateral hemisphere ( $p < 0.05$ ). In addition, the cytochrome oxidase activity in the contralateral hemisphere was 15% lower in the Rot/MB group than in the Rot group ( $p < 0.05$ ) ([Table 1](#)).

Table 1

Mean total striatal mitochondrial complex I and cytochrome oxidase activity after unilateral lesions

	Rot	Rot/MB	Group effect (p value)
<b>NADH dehydrogenase (complex I) activity (nmoles/min/mg)</b>			
Total ipsilateral	1014 ± 5	1111 ± 6	0.27
Total contralateral	1286 ± 5	1306 ± 4	0.77
<i>Within-group difference (%)</i>	<b>-21.1**</b>	<b>-14.9*</b>	0.34
<b>Cytochrome oxidase (complex IV) activity (µmoles/min/g)</b>			
Total ipsilateral	309 ± 8	288 ± 12	0.59
Total contralateral	287 ± 12	244 ± 12	<b>0.021</b>
<i>Within-group difference (%)</i>	7.6	<b>18*</b>	0.06

\* significant within-group difference,  $p < 0.05$

\*\* significant within group difference,  $p < 0.01$

Isolated striatal mitochondria were used to further analyze the specific interactions of Rot and MB with mitochondrial complex I *in vitro*. A 63% decrease in complex I activity relative to control was detected in striatal mitochondria as early as 3 min after incubation with Rot ( $1.5 \pm 0.3$  µmoles/min/mg, control vs. 0.5 µmoles/min/mg rotenone,  $p < 0.05$ ). An MB concentration estimated to be similar to those reached in the striatum after *in vivo* infusion did not prevent the inhibitory effect of Rot on complex I. In fact, MB concentrations 10 and 100 times higher were also ineffective at increasing complex I activity in the presence of Rot ([Fig. 5](#)). These data exclude the possibility that MB reacts with Rot or blocks its binding site at complex I. In addition, by being detectable after only several min of incubation, this *in vitro* inhibitory effect of Rot on complex I activity supports an early metabolic compromise previous to neurodegeneration.

## [Figure 5](#)

### **Rotenone induces complex I dysfunction in striatal mitochondria not reversible by methylene blue**

Compared to control, striatal mitochondria exposed to rotenone (Rot) showed a 63% decrease in complex I activity after only 3 min. MB concentrations estimated to be similar to those reached after *in vivo* infusion (0.5  $\mu$ M) did not prevent Rot effects. High MB concentrations (5  $\mu$ M and 50  $\mu$ M) were also ineffective at preventing the Rot-induced complex I activity inhibition, which rules out the possibility that the neuroprotective effects of MB are due to a direct interaction with rotenone molecules or to blockade of Rot's binding site at complex I. \* = different than control,  $p < 0.05$ .

### **MB protected against the motor network impairments outside the striatal lesion**

MB also produced differential effects on the metabolic activity of several motor control-related regions. Thus, a 7% higher cytochrome oxidase activity was found in the SNc ipsilateral to the striatal infusion of Rot/MB, compared to that found in the SNc ipsilateral to the striatal infusion of Rot without MB ( $p < 0.05$ ). Moreover, rats in the Rot/MB showed a significant increase in the metabolic activity of the ipsilateral CPuR (15.4%), PPTg (5.4%) and MO (3.5%), but such changes were not observed in the Rot group. Compared to contralateral structures, increases in metabolic activity in the ipsilateral SNr, SNc, CPuC, as well as in thalamic and cortical regions involved in motor control, were common to both groups.

Further effects of MB on cerebral metabolic activity were revealed by the analysis of metabolic mapping data in terms of interregional correlations of cytochrome oxidase activity. Rot induced a general weakening of functional connectivity in the basal ganglia-thalamocortical motor loop compared to control, whereas subjects in the Rot/MB group showed evidence of strong global functional coupling that was significantly different from Rot subjects and more similar to control. In both the control and Rot/MB groups, functional coupling appeared strengthened in the indirect nigrostriatal pathway, as well as in the thalamo-cortical and cortical-striatal connections ([Fig. 6](#)).

## [Figure 6](#)

### **Methylene blue enhances the functional connectivity between regions involved in motor control**

The cytochrome oxidase activity data from the lesioned hemispheres were applied to an anatomical network model of motor control, and patterns of functional connectivity were determined based on interregional metabolic activity correlations. The vehicle-injected control group was used as a reference for functional connectivity in the network of interest. The striatal damage induced by rotenone (Rot) resulted in a general functional disconnection (thinner arrows) in the basal ganglia-thalamocortical motor loop, with a pattern characterized by 1) decoupling between the subthalamic nucleus (STh) and the substantia nigra reticulata (SNr), 2) decoupling between thalamic regions (VA/VL) and the secondary motor cortex (M2), 3) decoupling between M2 and the striatum (CPu), and 4) emergence of a strong functional correlation between CPu and SNr (i.e. descending striatonigral pathway). MB co-treated subjects (Rot/MB) showed strengthening of functional influences in the indirect striatal, thalamocortical and corticostriatal pathways compared to Rot, a pattern suggestive of MB-induced network normalization that was similar to control. Arrow direction is given by the anatomical connectivity model and arrow thicknesses represent the magnitude of the interregional correlation coefficients ( $r$ ) (i.e. an index of the degree of functional coupling). Thicker lines represent higher functional coupling, whereas thinner lines represent lower coupling. Solid arrows represent positive (+ $r$ ), whereas segmented arrows represent negative ( $-r$ ) interregional metabolic activity correlations. \* = significant difference from control. • = significant difference from Rot group.

### **MB prevented the behavioral deficits elicited by striatal damage**

MB co-administration partially prevented the behavioral asymmetries induced in rats by the unilateral infusion of Rot in the striatum. This effect was particularly evident in the dot removal test ([Table 2](#)). Subjects in the Rot group displayed an ipsilateral bias in the order of dot removal, namely they would first contact and remove the stimulus placed on their unimpaired (ipsilateral) forelimb. This was quantified by a 65.5% decrease in the post-infusion dot removal rate from the impaired (contralateral) limb, compared to pre-infusion performance in Rot-treated animals. Notably, such a bias appeared significantly reduced in the Rot/MB group, where the reduction in the rate of dot removal from pre-infusion performance was only 34.7%. Furthermore, MB co-administration counteracted the increase in the latency to contact the stimulus placed on the impaired (contralateral) forelimb caused by Rot, as no significant changes in this parameter were observed in the Rot/MB group. The results observed in the vibrissae-evoked placing test corroborate the dot test findings, as subjects in the Rot/MB group displayed no significant difference in placing performance as compared to pre-infusion levels, whereas this parameter was significantly impaired in Rot-treated rats. Finally, no between-group and within-group differences were detected in any of the open field measured parameters. None of the behavioral tests showed differences in the use of the unimpaired (ipsilateral) limb between pre- and post-infusion in either the Rot or Rot/MB-treated groups. This observation supports the suitability of these tests to investigate motor asymmetries and potential agents capable of counteracting their onset.

## Table 2

Behavioral asymmetries following unilateral intrastriatal lesions

<b>Behavioral test</b>	<b>Rot</b>	<b>Rot/MB</b>	<b>Group effect (p value)</b>
<b>Dot test</b>			
Difference (%) between pre- and post- lesion trials in which the contra dot was removed before the ipsi dot	<b>-65.6*</b>	<b>-34.7*</b>	<b>0.03**</b>
Latencies (sec)			
Contralateral contact			
Pre-lesion	3.7 ± 0.5	4.6 ± 1	
Post-lesion	15.9 ± 6	4.8 ± 0.6	
<i>Difference</i>	<b>12.2*</b>	0.2	<b>0.01**</b>
Ipsilateral contact			
Pre-lesion	4.9 ± 0.8	5.4 ± 1	
Post-lesion	9.6 ± 6	3.6 ± 0.4	
<i>Difference</i>	4.7	-1.8	0.88
Contralateral removal			
Pre-lesion	8.7 ± 2	9.3 ± 1	
Post-lesion	32.1 ± 7	22 ± 6	
<i>Difference</i>	<b>23.4*</b>	<b>12.7*</b>	0.24
Ipsilateral removal			
Pre-lesion	14.3 ± 4	11 ± 2	
Post-lesion	19.8 ± 7	4.6 ± 0.7	
<i>Difference</i>	5.5	-6.4	0.74
<b>Vibrissae-evoked placing test (score)</b>			
Contralateral			
Pre-lesion	3	3	

\* significant within-group difference, p < 0.05

\*\* significant within-group difference, p < 0.01

The protective effects of MB co-administration against Rot-induced behavioral motor asymmetries are further supported by the presence of between-group differences in brain-behavior correlations. No significant correlations between the total striatal metabolic activity and contralateral difference scores in the behavioral tests were observed in the Rot group. In contrast, in the MB-treated group, striatal metabolic activity

correlated with the contralateral dot removal difference score ( $r = 0.74$ ,  $p < 0.05$  vs.  $r = 0.19$ ,  $p = 0.65$  in the Rot group) and with the contralateral vibrissae-stimulation evoked placing difference score ( $r = -0.79$ ,  $p < 0.01$  vs.  $r = 0.56$ ,  $p = 0.14$  in the Rot group).

### MB also showed neuroprotective effects in a bilateral striatal infusion model

In the bilateral infusion model, MB co-administration produced a 73.5% reduction in the mean striatal lesion volume induced by Rot ( $p < 0.01$ ), compared to the Rot alone-treated hemispheres (Fig. 7). Striatal lesions in Rot-treated hemispheres showed a total average volume of  $35.2 \pm 7 \text{ mm}^3$  which occupied  $7 \pm 1\%$  of the total striatum volume. Similar to the unilateral model, the lesions featured an area of liquefactive necrosis. In contrast, the contralateral hemispheres, in which Rot/MB was infused, displayed a mean average lesion volume of only  $9.3 \pm 4 \text{ mm}^3$ , which represents only  $2 \pm 1\%$  of the total striatum volume. In addition, the neuropathologic features of the lesions in the Rot/MB group were less severe than in the Rot group. There were no interhemispheric differences in total striatal volume ( $483.5 \pm 32 \text{ mm}^3$ , left vs.  $481.4 \pm 47 \text{ mm}^3$ , right,  $p = 0.97$ ).

#### [Figure 7](#)

##### **Effects of methylene blue co-administration on the neuronal damage induced by bilateral intrastratial infusions of rotenone**

(A) Nissl-stained forebrain coronal section of a subject receiving bilateral intrastratial infusions of rotenone alone (Rot, left hemisphere) and rotenone plus MB (Rot/MB, right hemisphere). The Rot-treated hemisphere showed an ellipsoidal mid-striatal lesion, characterized by a cavity of liquefactive necrosis surrounded by a rim of reactive gliosis (asterisk). The lesion was accompanied by callosal damage and hydrocephalus (black arrow). In contrast, the MB co-treated hemisphere showed significantly less striatal damage, featuring a comparatively smaller lesion limited to the corpus callosum (white arrow). (B) Within-subject mean lesion volume difference. MB co-treatment significantly decreased the total striatal lesion volume, compared to the Rot alone-treated hemisphere. \*\* =  $p < 0.01$ .

## DISCUSSION

---

The present study demonstrates for the first time that MB exerts protective effects against structural, neurochemical and behavioral deficits induced by the direct intrastratial infusion of Rot in rats. The anatomicopathologic features of the damage produced by the intrastratial injection of Rot observed in this study (i.e., liquefactive necrosis and reactive gliosis) are akin to those peculiar to the lesions described in patients with certain types of inborn errors of metabolism ([Heidenreich et al., 1988](#), [Roodhooft et al., 1990](#)). These lesions have been reported to be a form of neurotoxic degeneration independent from hypoxemia and/or vascular deficiency. Rather they stem from the neurotoxic effects elicited by accumulating organic acid metabolites, which eventually lead to mitochondrial dysfunction ([Brismar and Ozand, 1994](#), [Gascon et al., 1994](#), [Okun et al., 2002](#)). Such lesions consist of foci of necrosis, gliosis and spongiosis that appear as bi-

lateral hypodensities, T<sub>2</sub> hyperintensities and atrophy of the striatum, putamen or globus pallidus ([Korf et al., 1986](#), [Brismar and Ozand, 1994](#), [Gascon et al., 1994](#)). The current study presents evidence supporting that similar degenerative changes can be induced by the infusion of the neurotoxin Rot.

Rot has been classically characterized as a selective inhibitor of mitochondrial complex I ([Palmer et al., 1968](#), [Gutman et al., 1970](#), [Greenamyre et al., 2001](#)). Its neurotoxic mechanism of action in striatal cells has been shown to be related to production of reactive oxygen species ([Moldzio et al., 2008](#)). Complex I has been regarded as a major source of reactive oxygen species, especially when its function is inhibited by Rot ([Lenaz et al., 2006](#)). In line with this, neural cells transfected with Rot-insensitive single-subunit complex I do not display mitochondrial impairment, oxidative damage, or death ([Sherer et al., 2003](#)), which supports that Rot-induced increases in oxidative stress are secondary to complex I inhibition. Nevertheless, dopaminergic cells from knockout mice deficient in functional complex I showed no increases in cell death, and in fact were more sensitive to Rot toxicity ([Choi et al., 2008](#)). Hence, although Rot might induce neurodegeneration *via* inhibition of complex I with a concomitant increase in oxidative stress, alternate neurotoxic mechanisms and sources of oxidative stress secondary to Rot exposure seem to be possible. Rot-induced oxidative damage lowers the threshold for activation of mitochondrial-dependent apoptosis and makes compromised neurons more likely to degenerate ([Perier et al., 2005](#)). In this study we provide evidence that both increases in oxidative stress and impairment in mitochondrial respiration are associated with Rot-induced striatal damage. Similar to what has been previously shown with whole brain mitochondria ([Rojas et al., 2009](#)), isolated striatal mitochondria incubated with Rot manifested an immediate compromise of complex I activity. Rot also induced early decrease in striatal energy metabolism capacity *in vivo* and induced increases in perilesional striatal superoxide levels.

A first clear effect of MB observed in the present study was its ability to visibly reduce the extent of Rot-induced striatal degeneration, an effect that was evident in the bilateral and unilateral models of Rot-induced damage. Co-administration of MB displayed a series of metabolic effects that were not restricted to the core of the Rot-induced lesion, but were extended to the lesion penumbra, the contralateral striatum and distant motor regions. At the lesion core, MB prevented the decrease in cytochrome oxidase activity induced by Rot, supporting a metabolic enhancing effect. On the other hand, MB actually showed a paradoxical decreased in cytochrome oxidase activity in the lesion penumbra. The penumbra displays peculiar neurochemical conditions including impaired electric conduction, glutamate receptor hyperactivation, calcium overload, increased oxidative stress and damage to the neurovascular matrix, that render it different from the surrounding spared tissue ([Lo, 2008](#)). We observed increases in penumbral oxidative stress in the Rot group that were decreased in the Rot/MB group, evidencing the antioxidant effects of MB. The combined effects of MB on perilesional oxidative stress and cytochrome oxidase activity support a mechanism in which an antioxidant effect parallels decreases in excitotoxicity that underlie prevention of structural damage.

In *in vitro* experiments with striatal mitochondria, MB treatment showed no effect on Rot-induced inhibition of complex I activity, and there were no between-group differences in *in situ* striatal complex I activity. These results suggest that MB's neuroprotection in the striatum is likely not mediated by direct enhancement of complex I activity. The data also rule out the possible molecular interaction of MB with Rot as a mechanism mediating neuroprotection. In addition, chromatographic analyses have shown that Rot and MB do not interact chemically when both are present in the same solution ([Zhang et al., 2006](#)). However, we found that MB boosted ipsilateral striatal metabolic capacity as measured with cytochrome oxidase ac-

tivity, compared to the contralateral striatum. MB studies in our laboratory were the first to show that MB increases brain oxygen consumption ([Riha et al., 2005](#), [Zhang et al., 2006](#)) and brain cytochrome oxidase activity both *in vitro* and *in vivo* ([Callaway et al., 2004](#), [Gonzalez-Lima and Bruchey, 2004](#), [Wrubel et al., 2007](#)), and improves brain function *in vivo* in the presence of sodium azide, a cytochrome oxidase inhibitor ([Callaway et al., 2002](#)). [Atamna et al. \(2008\)](#) also showed in fibroblasts in tissue culture that MB delays cell senescence by increasing oxygen consumption and preventing the formation of oxidants through cycling of MB between oxidized and reduced forms. Therefore, based on the above observations, it can be hypothesized that the antioxidant and metabolic effects of MB could impact neuronal survival.

Of relevance to the understanding of the potential protective effects of MB on brain function under toxic conditions is the finding that the modulation of metabolic activity by MB was not restricted to the lesion and its vicinity. Conversely, a decreased metabolic activity in the contralateral striatum was observed in the Rot/MB group but not in the Rot group, a finding that supports the ability of MB co-administration in counteracting contralateral compensatory responses produced by Rot-induced lesions. Furthermore, MB co-administration was found to influence the metabolic activity in both close and remote structures of a neural network involved in motor control. Indeed, it was observed that the presence of a striatal lesion induced a marked ipsilateral activation of basal ganglia regions, thalamus and cortex in both the Rot- and Rot/MB-treated subjects. However, the patterns of combined activation in both groups were different. Thus, brains in the Rot group featured a functionally decoupled ipsilateral motor network, an effect that was prevented in Rot/MB brains, as demonstrated by the high interregional correlations observed in this group. To correctly interpret the previous data, it is important to highlight that the reported interregional correlations do not depend on the type of online and task-dependent regional activation, as observed with other functional neuroimaging modalities like fMRI or PET. Instead, the metabolic mapping method based on cytochrome oxidase activity likely reflects long-lasting changes in brain metabolic capacity determined by sustained energy demands ([Sakata et al., 2000](#), [Sakata et al., 2005](#)). Therefore, the observed between-group differences in regional brain metabolism provide evidence that MB co-administration counteracts the neurotoxicity of Rot not only by limiting its deleterious effects on brain structure but also by triggering potentially advantageous functional network changes in brain metabolism, which may contribute to adaptive rewiring ([Dancause et al., 2005](#)).

The protective effects of MB against Rot-induced striatal damage were also observed at the behavioral level. A beneficial effect of MB against Rot-induced behavioral impairment was observed in the dot removal test where MB co-administration attenuated the bias in the removal of the contralateral dot, as well as the decrease in latency to contralateral dot contact observed in Rot-treated rats. Similarly, the vibrissae stimulation-evoked placing test also revealed within-group score decrements in Rot-treated rats that were not observed in Rot/MB-treated rats. Thus these two behavioral tests showed sensitivity not only to the onset and severity of motor asymmetries, but also to differences between highly impaired subjects (i.e. in the Rot group) and mildly impaired subjects (i.e. in the Rot/MB group).

The findings are consistent with MB's protection against Rot neurotoxicity found in the retina previously ([Zhang et al., 2006](#), [Rojas et al., 2009](#)) and further support the possibility that MB may exert its neuroprotective effects *in vivo* by means of a dual molecular mechanism implicating both antioxidant and metabolic enhancing effects on mitochondrial respiration. Given that Rot-induced neurodegeneration is particularly contingent on increases of oxidative stress as opposed to bioenergetic failure alone ([Sherer et al., 2003](#)), the tissue sparing effects of MB can be attributed mainly to its powerful antioxidant effects. Indeed, imino-

containing compounds such as MB are known to have superior antioxidant properties compared to vitamin E and phenolic compounds ([Moosmann et al., 2001](#)). Nevertheless, MB's unique chemical structure, featuring a central thiazine ring, allows it to be not only very susceptible to reduction, but at the same time easily auto-oxidized, depending on MB's concentration and the redox conditions of the milieu. *In vivo*, at low MB concentrations such as used in this study, oxidized and reduced forms of MB are at equilibrium, and function as a reversible redox system ([Bruchey and Gonzalez-Lima, 2008](#)) with powerful antioxidant and respiratory enhancing effects ([Zhang et al., 2006](#)). Thus, MB can enter a cycle of oxidation and reduction which eventually can prevent oxidative damage and sustain mitochondrial function. These respiratory enhancing effects of MB appear related to the generalized brain network and behavioral effects detected in this study.

The present findings support that MB could be a valuable intervention against neural damage associated with oxidative stress and energy hypometabolism. They also add to our previous work evidencing a possible therapeutic role of interventions targeting mitochondrial function in neurodegenerative disorders ([Rojas et al., 2008a](#), [Pienaar et al., 2009](#)). It is important to notice, however, that the co-administration paradigm used in this study is limited in its capacity to reveal the potential neuroprotective value of MB after the onset of neurodegeneration or as an effective prophylactic intervention before neurodegeneration is evident. Thus, the effects of MB should be further investigated in paradigms that address these two conditions that are highly relevant for clinical applications. This implies a specific focus on the effects of pre-lesion and post-lesion as well as systemic MB administration.

## CONCLUSION

---

This study provides the first demonstration of the anatomical, metabolic and behavioral neuroprotective effects of methylene blue in the striatum *in vivo*. Co-administration of MB provided effective protection against striatal structural damage and oxidative stress. MB also improved brain metabolic activity and some features of behavioral impairment elicited by infusion of the mitochondrial toxin Rot in the striatum. Further testing of MB is indicated to help determine its potential value as an effective neuroprotective intervention in clinical conditions associated with oxidative damage and energetic failure.

## ACKNOWLEDGMENTS

---

Supported in part by NIH Grant MH65728 to Prof. F. Gonzalez-Lima and CONACYT 187413 to Dr. Julio C. Rojas. Dr. Nicola Simola is supported by funds from "Regione Autonoma della Sardegna" for the international mobility of young researchers (Project "Master and Back"). We thank Genevieve M. Holmes for her help with brain extractions and mitochondria isolation.

## Abbreviations

---

ANOVA	Analysis of variance
ACC	Anterior cingulate cortex
CPuC	Caudal Striatum
CM	Centromedian thalamic nucleus
DHE	Dihydroethidium
DMSO	Dymethylsulfoxide
LGP	Lateral globus pallidus
MFC	Medial frontal cortex
MO	Medial orbital cortex
MB	Methylene blue
NADH	Nicotinamide adenine dinucleotide
PTTg	Pedunculopontine nucleus
PB	Phosphate buffer
CPuR	Rostral striatum
Rot	Rotenone
M2	Secondary motor cortex
CPu	Striatum
SNc	Substantia nigra compacta
SNr	Substantia nigra reticulata
STh	Subthalamic nucleus

VA	Ventral anterior thalamic nucleus
VL	Ventrolateral thalamic nucleus

## Footnotes

---

**Publisher's Disclaimer:** This is a PDF file of an unedited manuscript that has been accepted for publication. As a service to our customers we are providing this early version of the manuscript. The manuscript will undergo copyediting, typesetting, and review of the resulting proof before it is published in its final citable form. Please note that during the production process errors may be discovered which could affect the content, and all legal disclaimers that apply to the journal pertain.

## REFERENCES

---

1. Alam M, Mayerhofer A, Schmidt WJ. The neurobehavioral changes induced by bilateral rotenone lesion in medial forebrain bundle of rats are reversed by L-DOPA. *Behav Brain Res.* 2004;151:117–124. [[PubMed](#)] [[Google Scholar](#)]
2. Alexander GE, Crutcher MD, DeLong MR. Basal ganglia-thalamocortical circuits: parallel substrates for motor, oculomotor, “prefrontal” and “limbic” functions. *Prog Brain Res.* 1990;85:119–146. [[PubMed](#)] [[Google Scholar](#)]
3. Anstrom KK, Schallert T, Woodlee MT, Shattuck A, Roberts DC. Repetitive vibrissae-elicited forelimb placing before and immediately after unilateral 6-hydroxydopamine improves outcome in a model of Parkinson’s disease. *Behav Brain Res.* 2007;179:183–191. [[PubMed](#)] [[Google Scholar](#)]
4. Atamna H, Nguyen A, Schultz C, Boyle K, Newberry J, Kato H, Ames BN. Methylene blue delays cellular senescence and enhances key mitochondrial biochemical pathways. *FASEB J.* 2008;22:703–712. [[PubMed](#)] [[Google Scholar](#)]
5. Barth TM, Stanfield BB. Homotopic, but not heterotopic, fetal cortical transplants can result in functional sparing following neonatal damage to the frontal cortex in rats. *Cereb Cortex.* 1994;4:271–278. [[PubMed](#)] [[Google Scholar](#)]
6. Brismar J, Ozand PT. CT and MR of the brain in the diagnosis of organic acidemias. Experiences from 107 patients. *Brain Dev.* 1994;(16 Suppl):104–124. [[PubMed](#)] [[Google Scholar](#)]
7. Bruchey AK, Gonzalez-Lima F. Behavioral, physiological and biochemical hormetic responses to the autoxidizable dye methylene blue. *Am J Pharm & Toxicol.* 2008;3:69–76. [[PMC free article](#)] [[PubMed](#)] [[Google Scholar](#)]
8. Callaway NL, Riha PD, Bruchey AK, Munshi Z, Gonzalez-Lima F. Methylene blue improves brain oxidative metabolism and memory retention in rats. *Pharmacol Biochem Behav.* 2004;77:175–181. [[PubMed](#)] [[Google Scholar](#)]
9. Callaway NL, Riha PD, Wrubel KM, McCollum D, Gonzalez-Lima F. Methylene blue restores spatial memory retention impaired by an inhibitor of cytochrome oxidase in rats. *Neurosci Lett.* 2002;332:83–86. [[PubMed](#)] [[Google Scholar](#)]
10. Choi WS, Kruse SE, Palmiter RD, Xia Z. Mitochondrial complex I inhibition is not required for dopaminergic neuron death induced by rotenone, MPP+, or paraquat. *Proc Natl Acad Sci U S A.* 2008;105:15136–15141. [[PMC free article](#)] [[PubMed](#)] [[Google Scholar](#)]

11. Clifton J, 2nd, Leikin JB. Methylene blue. *Am J Ther.* 2003;10:289–291. [[PubMed](#)] [[Google Scholar](#)]
12. Dancause N, Barbay S, Frost SB, Plautz EJ, Chen D, Zoubina EV, Stowe AM, Nudo RJ. Extensive cortical rewiring after brain injury. *J Neurosci.* 2005;25:10167–10179. [[PMC free article](#)] [[PubMed](#)] [[Google Scholar](#)]
13. Estornell E, Fato R, Pallotti F, Lenaz G. Assay conditions for the mitochondrial NADH:coenzyme Q oxidoreductase. *FEBS Lett.* 1993;332:127–131. [[PubMed](#)] [[Google Scholar](#)]
14. Fleming SM, Delville Y, Schallert T. An intermittent, controlled-rate, slow progressive degeneration model of Parkinson's disease: antiparkinson effects of Sinemet and protective effects of methylphenidate. *Behav Brain Res.* 2005;156:201–213. [[PubMed](#)] [[Google Scholar](#)]
15. Furian AF, Figuera MR, Oliveira MS, Ferreira AP, Fiorenza NG, de Carvalho Myskiw J, Petry JC, Coelho RC, Mello CF, Royes LF. Methylene blue prevents methylmalonate-induced seizures and oxidative damage in rat striatum. *Neurochem Int.* 2007;50:164–171. [[PubMed](#)] [[Google Scholar](#)]
16. Gascon GG, Ozand PT, Brismar J. Movement disorders in childhood organic acidurias. Clinical, neuroimaging, and biochemical correlations. *Brain Dev.* 1994;(16 Suppl):94–103. [[PubMed](#)] [[Google Scholar](#)]
17. Gonzalez-Lima F, Bruchey AK. Extinction memory improvement by the metabolic enhancer methylene blue. *Learn Mem.* 2004;11:633–640. [[PMC free article](#)] [[PubMed](#)] [[Google Scholar](#)]
18. Gonzalez-Lima F, Cada A. Cytochrome oxidase activity in the auditory system of the mouse: a qualitative and quantitative histochemical study. *Neuroscience.* 1994;63:559–578. [[PubMed](#)] [[Google Scholar](#)]
19. Gonzalez-Lima F, Cada A. Quantitative histochemistry of cytochrome oxidase activity: Theory, methods, and regional brain vulnerability. In: Gonzalez-Lima F, editor. *Cytochrome oxidase in neuronal metabolism and Alzheimer's disease*. New York: Plenum press; 1998. pp. 55–90. [[Google Scholar](#)]
20. Gonzalez-Lima F, Jones D. Quantitative mapping of cytochrome oxidase activity in the central auditory system of the gerbil: a study with calibrated activity standards and metal-intensified histochemistry. *Brain Res.* 1994;660:34–49. [[PubMed](#)] [[Google Scholar](#)]
21. Grafton ST, Sutton J, Couldwell ML, Waters C. Network analysis of motor system connectivity in Parkinson's disease: modulation of thalamocortical interactions after pallidotomy. *Hum Brain Mapp.* 1994;2:45–55. [[Google Scholar](#)]
22. Greenamyre JT, Sherer TB, Betarbet R, Panov AV. Complex I and Parkinson's disease. *IUBMB Life.* 2001;52:135–141. [[PubMed](#)] [[Google Scholar](#)]
23. Gutman M, Singer TP, Beinert H, Casida JE. Reaction sites of rotenone, piericidin A, and amytal in relation to the nonheme iron components of NADH dehydrogenase. *Proc Natl Acad Sci U S A.* 1970;65:763–770. [[PMC free article](#)] [[PubMed](#)] [[Google Scholar](#)]
24. Heidenreich R, Natowicz M, Hainline BE, Berman P, Kelley RI, Hillman RE, Berry GT. Acute extrapyramidal syndrome in methylmalonic acidemia: "metabolic stroke" involving the globus pallidus. *J Pediatr.* 1988;113:1022–1027. [[PubMed](#)] [[Google Scholar](#)]
25. Hua Y, Schallert T, Keep RF, Wu J, Hoff JT, Xi G. Behavioral tests after intracerebral hemorrhage in the rat. *Stroke.* 2002;33:2478–2484. [[PubMed](#)] [[Google Scholar](#)]
26. Jones D, Gonzalez-Lima F. Associative effects of Pavlovian differential inhibition of behaviour. *Eur J Neurosci.* 2001;14:1915–1927. [[PubMed](#)] [[Google Scholar](#)]

27. Jung C, Higgins CM, Xu Z. A quantitative histochemical assay for activities of mitochondrial electron transport chain complexes in mouse spinal cord sections. *J Neurosci Methods*. 2002;114:165–172. [[PubMed](#)] [[Google Scholar](#)]
28. Korf B, Wallman JK, Levy HL. Bilateral lucency of the globus pallidus complicating methylmalonic acidemia. *Ann Neurol*. 1986;20:364–366. [[PubMed](#)] [[Google Scholar](#)]
29. Kupfer A, Aeschlimann C, Cerny T. Methylene blue and the neurotoxic mechanisms of ifosfamide encephalopathy. *Eur J Clin Pharmacol*. 1996;50:249–252. [[PubMed](#)] [[Google Scholar](#)]
30. Kupfer A, Aeschlimann C, Wermuth B, Cerny T. Prophylaxis and reversal of ifosfamide encephalopathy with methylene-blue. *Lancet*. 1994;343:763–764. [[PubMed](#)] [[Google Scholar](#)]
31. Lehninger AL. *Molecular basis of structure and function*. New York: W.A: Benjamin, Inc; 1964. The mitochondrion. [[Google Scholar](#)]
32. Lenaz G, Fato R, Genova ML, Bergamini C, Bianchi C, Biondi A. Mitochondrial Complex I: structural and functional aspects. *Biochim Biophys Acta*. 2006;1757:1406–1420. [[PubMed](#)] [[Google Scholar](#)]
33. Lindahl PE, Oberg KE. The effect of rotenone on respiration and its point of attack. *Exp Cell Res*. 1961;23:228–237. [[PubMed](#)] [[Google Scholar](#)]
34. Lo EH. A new penumbra: transitioning from injury into repair after stroke. *Nat Med*. 2008;14:497–500. [[PubMed](#)] [[Google Scholar](#)]
35. McIntosh AR, Gonzalez-Lima F. Structural modeling of functional neural pathways mapped with 2-deoxyglucose: effects of acoustic startle habituation on the auditory system. *Brain Res*. 1991;547:295–302. [[PubMed](#)] [[Google Scholar](#)]
36. Miculescu A, Basu S, Wiklund L. Methylene blue added to a hypertonic-hyperoncotic solution increases short-term survival in experimental cardiac arrest. *Crit Care Med*. 2006;34:2806–2813. [[PubMed](#)] [[Google Scholar](#)]
37. Moldzio R, Piskernik C, Radad K, Rausch WD. Rotenone damages striatal organotypic slice culture. *Ann N Y Acad Sci*. 2008;1148:530–535. [[PubMed](#)] [[Google Scholar](#)]
38. Moosmann B, Skutella T, Beyer K, Behl C. Protective activity of aromatic amines and imines against oxidative nerve cell death. *Biol Chem*. 2001;382:1601–1612. [[PubMed](#)] [[Google Scholar](#)]
39. Naylor GJ, Martin B, Hopwood SE, Watson Y. A two-year double-blind crossover trial of the prophylactic effect of methylene blue in manic-depressive psychosis. *Biol Psychiatry*. 1986;21:915–920. [[PubMed](#)] [[Google Scholar](#)]
40. O'Leary JL, Petty J, Harris AB, Inukai J. Supravital staining of mammalian brain with intra-arterial methylene blue followed by pressurized oxygen. *Stain Technol*. 1968;43:197–201. [[PubMed](#)] [[Google Scholar](#)]
41. Okun JG, Horster F, Farkas LM, Feyh P, Hinz A, Sauer S, Hoffmann GF, Unsicker K, Mayatepek E, Kolker S. Neurodegeneration in methylmalonic aciduria involves inhibition of complex II and the tricarboxylic acid cycle, and synergistically acting excitotoxicity. *J Biol Chem*. 2002;277:14674–14680. [[PubMed](#)] [[Google Scholar](#)]
42. Palmer G, Horgan DJ, Tisdale H, Singer TP, Beinert H. Studies on the respiratory chain-linked reduced nicotinamide adenine dinucleotide dehydrogenase. XIV. Location of the sites of inhibition of rotenone, barbiturates, and piericidin by means of electron paramagnetic resonance spectroscopy. *J Biol Chem*. 1968;243:844–847. [[PubMed](#)] [[Google Scholar](#)]
43. Paxinos G, Watson C. *The Rat Brain in Stereotaxic Coordinates*. San Diego: Academic Press; 1997. [[Google Scholar](#)]

44. Pelgrims J, De Vos F, Van den Brande J, Schrijvers D, Prove A, Vermorcken JB. Methylene blue in the treatment and prevention of ifosfamide-induced encephalopathy: report of 12 cases and a review of the literature. *Br J Cancer*. 2000;82:291–294. [[PMC free article](#)] [[PubMed](#)] [[Google Scholar](#)]
45. Perier C, Tieu K, Guegan C, Caspersen C, Jackson-Lewis V, Carelli V, Martinuzzi A, Hirano M, Przedborski S, Vila M. Complex I deficiency primes Bax-dependent neuronal apoptosis through mitochondrial oxidative damage. *Proc Natl Acad Sci U S A*. 2005;102:19126–19131. [[PMC free article](#)] [[PubMed](#)] [[Google Scholar](#)]
46. Peter C, Hongwan D, Kupfer A, Lauterburg BH. Pharmacokinetics and organ distribution of intravenous and oral methylene blue. *Eur J Clin Pharmacol*. 2000;56:247–250. [[PubMed](#)] [[Google Scholar](#)]
47. Pienaar IS, Schallert T, Hattingh S, Daniels WM. Behavioral and quantitative mitochondrial proteome analyses of the effects of simvastatin: implications for models of neural degeneration. *J Neural Transm*. 2009;116:791–806. [[PubMed](#)] [[Google Scholar](#)]
48. Riha PD, Bruchey AK, Echevarria DJ, Gonzalez-Lima F. Memory facilitation by methylene blue: dose-dependent effect on behavior and brain oxygen consumption. *Eur J Pharmacol*. 2005;511:151–158. [[PubMed](#)] [[Google Scholar](#)]
49. Rojas JC, John JM, Lee J, Gonzalez-Lima F. Methylene blue provides behavioral and metabolic neuroprotection against optic neuropathy. *Neurotox Res*. 2009;15:260–273. [[PubMed](#)] [[Google Scholar](#)]
50. Rojas JC, Lee J, John JM, Gonzalez-Lima F. Neuroprotective effects of near-infrared light in an in vivo model of mitochondrial optic neuropathy. *J Neurosci*. 2008a;28:13511–13521. [[PMC free article](#)] [[PubMed](#)] [[Google Scholar](#)]
51. Rojas JC, Saavedra JA, Gonzalez-Lima F. Neuroprotective effects of memantine in a mouse model of retinal degeneration induced by rotenone. *Brain Res*. 2008b;1215:208–217. [[PMC free article](#)] [[PubMed](#)] [[Google Scholar](#)]
52. Roodhooft AM, Baumgartner ER, Martin JJ, Blom W, Van Acker KJ. Symmetrical necrosis of the basal ganglia in methylmalonic acidemia. *Eur J Pediatr*. 1990;149:582–584. [[PubMed](#)] [[Google Scholar](#)]
53. Sakata JT, Coomber P, Gonzalez-Lima F, Crews D. Functional connectivity among limbic brain areas: differential effects of incubation temperature and gonadal sex in the leopard gecko, *Eublepharis macularius*. *Brain Behav Evol*. 2000;55:139–151. [[PubMed](#)] [[Google Scholar](#)]
54. Sakata JT, Crews D, Gonzalez-Lima F. Behavioral correlates of differences in neural metabolic capacity. *Brain Res Brain Res Rev*. 2005;48:1–15. [[PubMed](#)] [[Google Scholar](#)]
55. Saravanan KS, Sindhu KM, Mohanakumar KP. Acute intranigral infusion of rotenone in rats causes progressive biochemical lesions in the striatum similar to Parkinson's disease. *Brain Res*. 2005;1049:147–155. [[PubMed](#)] [[Google Scholar](#)]
56. Schallert T. Behavioral tests for preclinical intervention assessment. *NeuroRx*. 2006;3:497–504. [[PMC free article](#)] [[PubMed](#)] [[Google Scholar](#)]
57. Schallert T, Fleming SM, Leasure JL, Tillerson JL, Bland ST. CNS plasticity and assessment of forelimb sensorimotor outcome in unilateral rat models of stroke, cortical ablation, parkinsonism and spinal cord injury. *Neuropharmacology*. 2000;39:777–787. [[PubMed](#)] [[Google Scholar](#)]
58. Schallert T, Hernandez TD, Barth TM. Recovery of function after brain damage: severe and chronic disruption by diazepam. *Brain Res*. 1986;379:104–111. [[PubMed](#)] [[Google Scholar](#)]
59. Schallert T, Upchurch M, Lobaugh N, Farrar SB, Spirduso WW, Gilliam P, Vaughn D, Wilcox RE. Tactile extinction: distinguishing between sensorimotor and motor asymmetries in rats with unilateral nigrostriatal damage. *Pharmacol Biochem Behav*. 1982;16:455–462. [[PubMed](#)] [[Google Scholar](#)]

60. Schallert T, Upchurch M, Wilcox RE, Vaughn DM. Posture-independent sensorimotor analysis of inter-hemispheric receptor asymmetries in neostriatum. *Pharmacol Biochem Behav.* 1983;18:753–759. [[PubMed](#)] [[Google Scholar](#)]
61. Schallert T, Woodlee MT. *Motor systems: orienting and placing.* New York: Oxford University Press; 2005. [[Google Scholar](#)]
62. Scott A, Hunter FE., Jr Support of thyroxine-induced swelling of liver mitochondria by generation of high energy intermediates at any one of three sites in electron transport. *J Biol Chem.* 1966;241:1060–1066. [[PubMed](#)] [[Google Scholar](#)]
63. Sherer TB, Betarbet R, Testa CM, Seo BB, Richardson JR, Kim JH, Miller GW, Yagi T, Matsuno-Yagi A, Greenamyre JT. Mechanism of toxicity in rotenone models of Parkinson's disease. *J Neurosci.* 2003;23:10756–10764. [[PMC free article](#)] [[PubMed](#)] [[Google Scholar](#)]
64. Sindhu KM, Banerjee R, Senthilkumar KS, Saravanan KS, Raju BC, Rao JM, Mohanakumar KP. Rats with unilateral median forebrain bundle, but not striatal or nigral, lesions by the neurotoxins MPP+ or rotenone display differential sensitivity to amphetamine and apomorphine. *Pharmacol Biochem Behav.* 2006;84:321–329. [[PubMed](#)] [[Google Scholar](#)]
65. Sindhu KM, Saravanan KS, Mohanakumar KP. Behavioral differences in a rotenone-induced hemiparkinsonian rat model developed following intranigral or median forebrain bundle infusion. *Brain Res.* 2005;1051:25–34. [[PubMed](#)] [[Google Scholar](#)]
66. Taniwaki T, Okayama A, Yoshiura T, Togao O, Nakamura Y, Yamasaki T, Ogata K, Shigeto H, Ohyagi Y, Kira J, Tobimatsu S. Functional network of the basal ganglia and cerebellar motor loops in vivo: different activation patterns between self-initiated and externally triggered movements. *Neuroimage.* 2006;31:745–753. [[PubMed](#)] [[Google Scholar](#)]
67. Taniwaki T, Okayama A, Yoshiura T, Togao O, Nakamura Y, Yamasaki T, Ogata K, Shigeto H, Ohyagi Y, Kira J, Tobimatsu S. Age-related alterations of the functional interactions within the basal ganglia and cerebellar motor loops in vivo. *Neuroimage.* 2007;36:1263–1276. [[PubMed](#)] [[Google Scholar](#)]
68. Villalba RM, Lee H, Smith Y. Dopaminergic denervation and spine loss in the striatum of MPTP-treated monkeys. *Exp Neurol.* 2009;215:220–227. [[PMC free article](#)] [[PubMed](#)] [[Google Scholar](#)]
69. Wainwright M, Crossley KB. Methylene Blue--a therapeutic dye for all seasons? *J Chemother.* 2002;14:431–443. [[PubMed](#)] [[Google Scholar](#)]
70. Wischik CM, Bentham P, Wischik DJ, Seng KM. Tau aggregation inhibitor (TAI) therapy with rember™ arrests disease progression in mild and moderate Alzheimer's disease over 50 weeks. *Alzheimer's and Dementia.* 2008;4:T167. [[Google Scholar](#)]
71. Wong-Riley M. Changes in the visual system of monocularly sutured or enucleated cats demonstrable with cytochrome oxidase histochemistry. *Brain Res.* 1979;171:11–28. [[PubMed](#)] [[Google Scholar](#)]
72. Wong-Riley MT. Cytochrome oxidase: an endogenous metabolic marker for neuronal activity. *Trends Neurosci.* 1989;12:94–101. [[PubMed](#)] [[Google Scholar](#)]
73. Woodlee MT, Asseo-Garcia AM, Zhao X, Liu SJ, Jones TA, Schallert T. Testing forelimb placing “across the midline” reveals distinct, lesion-dependent patterns of recovery in rats. *Exp Neurol.* 2005;191:310–317. [[PubMed](#)] [[Google Scholar](#)]
74. Wrubel KM, Riha PD, Maldonado MA, McCollum D, Gonzalez-Lima F. The brain metabolic enhancer methylene blue improves discrimination learning in rats. *Pharmacol Biochem Behav.* 2007;86:712–717. [[PMC free article](#)] [[PubMed](#)] [[Google Scholar](#)]
75. Zhang X, Jones D, Gonzalez-Lima F. Mouse model of optic neuropathy caused by mitochondrial complex I dysfunction. *Neurosci Lett.* 2002;326:97–100. [[PubMed](#)] [[Google Scholar](#)]
76. Zhang X, Rojas JC, Gonzalez-Lima F. Methylene blue prevents neurodegeneration caused by rotenone in the retina. *Neurotox Res.* 2006;9:47–57. [[PubMed](#)] [[Google Scholar](#)]

